Constraints on climate sensitivity from temperature reconstructions of the past seven centuries

Gabriele C. Hegerl[1] , Thomas J. Crowley[1], William T. Hyde[1] and David J. Frame[2]

[1]*Division of Earth and Ocean Sciences, Nicholas School of the Environment and Earth Sciences, Duke University, Durham, North Carolina*

[2]*Climate Dynamics Group, Department of Physics, University of Oxford, UK*

Nature submission MS2005-07-07962B

The magnitude and impact of future global warming depends on the sensitivity of the climate system to changes in greenhouse gas concentrations. The commonly accepted range for the equilibrium global mean temperature change in response to a doubling of the atmospheric carbon dioxide concentration[1], termed climate sensitivity, is 1.5K to 4.5K[2]. However, a number of studies[3-10] find a substantial probability of significantly higher sensitivities, yielding observational upper 95% limits on climate sensitivity of 7.7K to above 9K[3-8]. Here we demonstrate that observational estimates of climate sensitivity can be tightened if reconstructions of northern hemispheric temperature over the last several centuries are considered. We use large-ensemble energy balance modelling to simulate the temperature response to past solar, volcanic, and greenhouse gas forcing and determine which climate sensitivities yield simulations that are in agreement with proxy reconstructions.

After accounting for the uncertainty in reconstructions and estimates of past external forcing, we find an independent estimate of climate sensitivity that is very similar to those from instrumental data. If the latter are combined with the result from all proxy reconstructions, then the 5-95% range shrinks to 1.5-6.2K, and to 1.5-4.6K when based on a reconstruction starting in AD 1500. This substantially reduces the probability of very high climate sensitivity.

We use four paleo reconstructions, namely a hemispheric reconstruction of mean annual temperatures by Mann and Jones[11], the maximum latewood density tree ring based reconstruction of Briffa *et al.*[12] for growing season temperatures over 20-90°N land, a revised and smoothed version of the Esper *et al.*[13] record that has been calibrated to 30-90N land annual data[14], and our own new decadal reconstruction termed "CH-blend" of annual average 30-90°N temperature[15] (Figure 1). A version of CH-blend using 12 records extends from 1505 to 1960; and a reconstruction based on 9 sites ("Ch-blend long") is used from 1270. Both reconstructions use a relatively small number of well spaced sites (often based on multiple records, including some regional reconstructions) throughout the reconstruction. CH-blend is consistent with independent estimates of temperatures from boreholes[15], and both CH-blend and CH-blend (long) agree well with

a recent reconstruction[16] that incorporates records of lower temporal resolution. The reconstruction method has been tested using noise-perturbed climate model data from the same locations as used in the reconstruction[15]. Results show that the reconstruction of decadal temperatures is accurate and reliably preserves hemispheric-scale temperature variability.

For CH-blend, our estimate of climate sensitivity fully accounts for the uncertainty in the amplitude of the record[15]. For the other reconstructions, we use both the published reconstruction and a version that is recalibrated using our technique. This approach avoids introducing a low bias in our estimate of climate sensitivity based on the possibility that some reconstruction techniques underestimate past climate variability[17] (for details see Supplementary Information).

We conduct a large ensemble (>1000) of simulations of the last thousand years with a 2.5-dimensional (latitude/longitude/depth) upwelling-diffusion energy balance model (EBM), with realistic land-sea distribution. The EBM is a variant of the seasonal model developed by North *et al.*[18] that simulates time-dependent responses to external forcing, and included the seasonal cycle (details see Supplementary Information). The same model has been previously used to examine the relationship between reconstructed temperature and external forcing over the past millennium[19,20]. EBM simulations reproduce the large-scale temperature response of general circulation models, and have the advantage of being able to generate large ensembles. The following two model parameters are important determinants of the large-scale response of climate models to external forcing[5] and have been systematically varied in our ensemble:

- Equilibrium climate sensitivity α, which was varied in 0.5K increments from 0.5K to 10.0K with an additional low value of 0.25K.

- Effective ocean diffusivity κ in the upwelling-diffusive model[21], which was varied between 0.63 and 3.8 cm^2/s. This range embraces an observational

estimate of 1.7+/- 0.2 cm^2/s based on a global compilation of GEOSECS data of bomb tritium penetration into the world ocean[22] and a lower range[23] based on bomb ^{14}C on the order of 1 cm^2/s. We have further tested our range of diffusivities by comparing simulated ocean warming with ocean heat content data from Levitus[24]. We find that the smaller to mid-range values of κ yield results that compare most favourably with these data, consistent with the observation that most of the 20th century increase in ocean heat content is in the upper 1000 m (Supplementary Figure 1). Note that ocean diffusivity is of smaller importance for the simulations of the preindustrial period, where forcings are mostly episodic and relatively small, than for the 20th century. In the latter period, the rate of temperature increase is crucially influenced by ocean diffusivity, since large diffusivities tend to hide more warming in the oceans than small diffusivities (see Supplementary Information for more discussion). Our results are insensitive to attempts to constrain κ further. They are, however, conditional on ocean effective diffusivity being within the range we use.

Prior work[19,20,25,15] has established that various reconstructions of hemispheric temperature consistently show influence from volcanism and greenhouse gas variations, and less consistently from variations in solar radiation. We force the EBM simulations with a combination of solar, volcanic, greenhouse gas, and tropospheric aerosol forcing to simulate hemispheric temperature change over the last millennium (Figure 2). Greenhouse gas forcing is based on changes in trace gases from ice core data, combined with IPCC estimates of radiative forcing for well-mixed greenhouse gases in the 20th century. The estimate of solar forcing is based on ^{14}C data[26], scaled to the Lean *et al.*[27] solar irradiance reconstruction after reducing its amplitude by 20% to accommodate recent conclusions that the former estimate may have been large[28]. For volcanism, we use an update of a global reconstruction[20] based on ice-core data from Greenland and Antarctica. We account for the considerable uncertainty in solar and volcanic forcing by varying the total amplitude of each forcing time-series around its central estimate. We use Monte Carlo simulations based on a 50% standard deviation for solar forcing, and a

35% standard deviation for volcanic forcing (excluding the unphysical case of net negative forcing). The uncertainty in our results due to random errors in the magnitude of individual volcanic eruptions was estimated by sensitivity tests, indicating that errors in the magnitude of individual eruptions can cause a modest widening of the tail of the distribution (Supplementary Figure 2, see Supplementary Information for more detail on forcings and their uncertainty).

We derive a probability density function (pdf) for climate sensitivity using a method related to one previously used for instrumental data[5,6] (see Method section and algorithm in Supplementary Information). Results for the CH-blend (short) reconstruction, for which we have the most reliable uncertainty estimate[15], yield a 5-95% range for sensitivity of 1.4K to 6.1K and a median sensitivity of 2.6K over the pre-instrumental period 1505-1850 (Figure 3a). Pdfs for climate sensitivity from the other reconstructions and the same period yield peak probabilities (modes) from 1.3K to 3.6K, and some of them suggest a moderate probability for climate sensitivity being high (see Supplementary Table 4). As expected, reconstructions with higher amplitudes of past climate fluctuations generally suggest higher climate sensitivities than those with low variability. The range of the other free parameters κ, and solar and volcanic forcing uncertainty, are used to fully explore uncertainties rather than to provide posterior information about best-fit values. Consistent with that, the preindustrial period does not provide constraints for ocean diffusivity, nor do results consistently favour a particular realization of forcing uncertainty, apart from a general preference for solar forcing on the low end of the range[19].

If all four reconstructions, both published and rescaled, are considered as equally likely realizations of the true hemispheric temperature evolution, the pdf that describes results from all four reconstructions combined yields a median sensitivity of 3.4K and a 5-95% range of 1.2K to 8.6K. This renders negative climate feedbacks to CO_2 changes

(corresponding to a climate sensitivity of under 1.1K) very unlikely. As in other estimates of climate sensitivity, the upper tail is not well constrained. Note that the upper limit of the transient climate response, which governs the near-term magnitude of the climate response, tends to be better constrained from observations than equilibrium climate sensitivity[8].

Our results are remarkably consistent with pdfs for climate sensitivity that have been estimated from the instrumental record[3-8] (Figure 3b) and that account for a differing level of uncertainty in forcings (most notably aerosol forcing[7]), ocean diffusivity, and observations. The response of climate to preindustrial forcing is governed (to a very reasonable approximation) by the same climate sensitivity. However, the uncertainties affecting each estimate are virtually independent, since the pre-industrial data are virtually independent from those for instrumental data from the second half of the 20th century (decadal data prior to that are used for calibrating the paleo data) and different forcing uncertainties affect each estimate. Therefore we can combine results from both to further constrain sensitivity. We use a version of the joint pdf for diffusivity and sensitivity, κ and α, from Frame *et al.*[8] that is based on decadal instrumental data from 1950 to 2000 as a prior probability (the use a prior pdf of κ and α combined accounts for their dependence; Supplementary Figure 5 shows a comparison between the published results for the entire 20th century[8] and the prior used here). We have widened the upper tail of the Frame *et al.* estimate in sensitivity in order to conservatively account for further uncertainties and embrace other instrumental estimates (results are only moderately sensitive to this, for details see Supplementary Information). Bayes' theorem is then used to calculate a posterior probability based on data from the past millennium (Figure 3c). The resulting 5-95% ranges for CH-blend (short) shrink to 1.6K to 4.6K, those for all proxy data combined to 1.5K to 6.2K. This result reduces the probability from 36% to 15% or less that climate sensitivity exceeds the upper limit of the IPCC range of 4.5K.

As previously shown, the agreement between models and data is mostly driven by the temperature response to volcanism, which causes longer-term variability due to the changing statistics of volcanic eruptions (Figure 2, see also Supplementary Table 3 for correlations between simulations and records on short and long timescales). A superposed epoch analysis previously showed that the EBM simulates the response-characteristics to volcanism very well[19]. The EBM does not simulate changes in atmospheric dynamics that have been associated with strong volcanic eruptions[29], but these changes do not much affect hemispheric and growing season or annually averaged temperatures[30].

We also caution that model uncertainties (beyond those that we account for) potentially affect all estimates of climate sensitivity. While our results are conditional on the range of effective ocean diffusivity and the upwelling parameter being realistic, simulated ocean heat content changes in our best-fit ocean simulation compare very well with recent data[24] (Supplementary Figure 1). Simulations with the most likely sensitivity of 2.5K also compare well to the low-frequency component of annual global temperatures from instrumental data (Supplementary Figure 4).

We conclude that proxy-reconstructions of the preindustrial period from 1270 to 1850 yield very similar estimates of climate sensitivity to those obtained from the virtually independent climate change over the 20th century. This agreement increases our confidence in the overall reliability of the estimates based on 20th century changes. When both independent lines of evidence are combined, the resulting pdf for climate sensitivity narrows, yielding a very small probability for climate sensitivity exceeding 7K (<3% based on all reconstructions combined, and <1% based on CH-blend).

METHODS:

ESTIMATING CLIMATE SENSITIVITY

Our method of estimating the probability density function of equilibrium climate sensitivity is related to a method used previously for instrumental data[5,6] and is briefly discussed here. A detailed algorithm can be found in the Supplementary Information. We simulate the time-space evolution of surface temperature over the last millennium forced with observed changes in solar, volcanic, greenhouse gas and sulfate aerosol forcing. We use a very large ensemble of EBM simulations with varying climate sensitivity α and ocean diffusivity κ, forced by different realizations of solar and volcanic forcing (f_{solar}, f_{volc}) to account for the most important uncertain parameters driving the simulated response. For the 20th century, aerosol forcing , f_{aer} is also varied. Each model simulation yields a time-space pattern of surface temperature response for each parameter $T(x,t,\alpha,\kappa,f_{sol},f_{vol},f_{aer})$. For each paleo reconstruction $\overline{T}_{paleo}$(overbar denoting a spatial average), the simulated spatial temperature patterns are averaged over the latitude strip and season the reconstruction is calibrated to, and filtered to the time-resolution used for the analysis (annual reconstructions are filtered by a 5-year running mean). All data are then centered from the beginning of the record to 1800 to focus on deviations from a mean climatic state of the past millennium and to exclude variations in the climate state caused by anthropogenic forcing. We analyze reconstructions from the beginning of the record, but not before A.D. 1270 (since there are significant uncertainties in the radiative forcing effects of a very large eruption in 1258). The analysis focuses on the residual between the simulated record $\overline{T}$ and the observed record

$$res(t,\alpha,\kappa,f_{sol},f_{vol},f_{aer}) = \overline{T}_{paleo}(t) - \overline{T}(t,\alpha,\kappa,f_{sol},f_{vol},f_{aer}). \quad (1)$$

Some combination of parameters will yield the residual with the smallest estimated variance $\hat{r}^2_{\min} = \min_{parameters}\left(\frac{\left\|(res(t,\alpha,\kappa,f_{sol},f_{vol},f_{aer}))\right\|^2}{n-1}\right)$, with

$\|res\|^2 = \sum_t res(t,\alpha,\kappa,f_{sol},f_{vol},f_{aer})^2$ and n denoting the length of the residual time series (yrs). The difference between any square residual $\|res\|^2$ and the minimum square residual $\|res_{\min}\|^2$ will then be F-distributed[5]

$$\frac{\|res(\alpha,\kappa,f_{aer},f_{sol},f_{vol})\|^2 - \|res_{\min}\|^2}{\hat{r}^2_{\min}} \sim mF(m,\nu). \quad (2)$$

where m is the number of free parameters (4 for the preindustrial case, 5 for the entire timeseries) and ν is the number of degrees of freedom in res_{min}. Note that for autocorrelated data, ν will be smaller than n. Therefore we account for the number of effectively independent samples in the square residual (see Supplementary Information). Thus, the likelihood of the reconstruction given each set of model parameters and forcings $p(data \mid \alpha,\kappa,f_{aer},f_{vol},f_{sol})$ is estimated from the probability that its residual variability is statistically indistinguishable from the best -fit residual[5], given internal climate variability and non-climatic random errors in proxy data.

Bayes theorem is used to derive the joint probability densitity function of the parameters

$$p(\alpha,\kappa,f_{aer},f_{vol},f_{sol} \mid data) \propto p(data \mid \alpha,\kappa,f_{aer},f_{vol},f_{sol}) \bullet p(\alpha,\kappa,f_{aer},f_{vol},f_{sol}) \quad (3)$$

from the likelihood of the data and the prior probability of the parameters $p(\alpha,\kappa,f_{aer},f_{vol},f_{sol})$. For results based on the proxy data alone, a uniform prior distribution for α is used for integration, which extends to a sensitivity of 10K and then drops off to zero. Similarly, a prior for κ is used that is uniform over the range we cover (see body of paper), and normal prior distributions are used for solar and volcanic uncertainty (see Figure 2). Where a prior distribution from the late 20th century is used, the joint probability density function p(α,κ) from Frame *et al.*[8] is applied instead of the uniform distribution.

This analysis is performed for every reconstruction. For reconstructions where the amplitude uncertainty can be fully accounted for (CH-blend and CH-blend long), this analysis is performed for the reconstruction scaled by a range of scaling factors β representing uncertainty in the amplitude of the reconstruction (see Supplementary Information). We use the best-guess scaling and the 2.5th, 10th, 25th, 75th, 90th and 97.5th percentile of β. All probability density functions resulting from these analyses $p(data(\beta) \mid \alpha, \kappa, f_{aer}, f_{vol}, f_{sol})$ are then averaged over β, weighted by the likelihood of each scaling β based on a normal distribution. This is a robust way of incorporating uncertainty in the reconstruction, since random errors in the reconstruction are directly accounted for in the residual. For reconstructions where the amplitude uncertainty cannot be fully estimated, we use both the published best guess and a rescaled best guess using our calibration method to estimate $p(data \mid \alpha, \kappa, f_{aer}, f_{vol}, f_{sol})$.

The resulting multi-dimensional likelihood is integrated over κ and forcing uncertainties f_{solar}, f_{volc}, and f_{aer}, yielding a probability density function for climate sensitivity. This is done both for each reconstruction individually, and for the average of the joint probabilities $p(\alpha, \kappa, f_{aer}, f_{vol}, f_{sol} \mid data)$ from all reconstructions to derive an estimate of climate sensitivity from all records combined.

Our method to estimate sensitivity has been validated using synthetic data (see Supplementary Figure 2), and tested by using an alternative method to estimate the likelihood based on scaling factors (see Supplementary Information).

Received:

1. Schneider, S. H. & Dickinson, R. E. Climate modeling. *Rev. Geophys. Space Phys.* **12**, 447 (1974).

2. Cubasch U. *et al*. Projections of Future Climate Change, in *Climate Change 2001: The Scientific Basis. Contribution of Working Group I to the Third Assessment Report of the Intergovernmental Panel on Climate Change* (Eds. Houghton, J. T. *et al*.) 525-582, Cambridge Univ. Press, New York (2001).

3. Andronova, N. G. & Schlesinger, M. E. Causes of global temperature changes during the 19th and 20th centuries. *Geophys. Res. Lett*. **27** (14), 2137-2140 (2000).

4. Gregory, J. M., Stouffer, R. J., Raper, S. C., Stott, P. A. & Rayner, N. A. An observationally based estimate of the climate sensitivity. *J. Climate*. **15**, 3117-3121 (2002).

5. Forest, C. E., Stone, P. H., Sokolov, A. P., Allen, M. R., & Webster, M. D. Quantifying uncertainties in climate system properties with the use of recent observations. *Science* **295**, 113 (2002).

6. Forest, C. E., Stone, P. H., and Sokolov, A. P. Estimated PDFs of climate system properties including natural and anthropogenic forcings. *Geophys. Res. Lett.,* in press (2006).

7. Knutti, R., Stocker, T. F., Joos, F. & Plattner, G.-K. Constraints on radiative forcing and future climate change from observations and climate model ensembles. *Nature* **416**, 719-723 (2002).

8. Frame, D. J. *et al*. Constraining climate forecasts: The role of prior assumptions. *Geophys. Rev. Lett.*, **32**, L09702, (2005).

9. Murphy, J. M. *et al*. Quantification of modelling uncertainties in a large ensemble of climate change simulations. *Nature* **430**, 768 (2004).

10. Stainforth, D. A. *et al*. Evaluating uncertainty in the climate response to changing levels of greenhouse gases. *Nature* **433**, 403 (2005).

11. Mann, M.E. & Jones, P.D. Global surface temperatures over the past two millennia. *Geophys. Res. Lett.,* **30**(15), 1820, doi:10.1029/2003GL017814 (2003).

12. Briffa, K. R. *et al*. Low-frequency temperature variations from a northern tree ring density network. *J. Geophys. Res.* **106**, 2929 (2001).

13. Esper, J., Cook, E. R. & Schweingruber, F. Low-frequency signals in long tree-ring chronologies for reconstructing past temperature variability. *Science* **295**, 2250-2253 (2002).

14. Cook, E., Esper, J. & D'Arrigo, R. Extra-tropical Northern Hemisphere land temperature variability over the past 1000 years. *Quat. Sci. Rev*. **23**, 2063-2074 (2004).

15. Hegerl, G. C. *et al*. Detection of human influence on a new, validated 1500 yr temperature reconstruction. *J. Climate*, submitted. (2006).

16. Moberg, A., Sonechkin, D. M., Holmgren, K., Datsenko, N. M. & Karlen, W. Highly variable Northern Hemisphere temperatures reconstructed from low- and high-resolution proxy data. *Nature* **433**, 613-617 (2005).

17. von Storch, H. et al. Reconstructing past climate from noisy data. *Science* **306**, 679-682, doi:10.1126/science.1096109 (2004).

18. North, G. R., Mengel, J. G. & Short, D. A simple energy balance model resolving the seasons and continents: Application to the astronomical theory of the ice ages. *J. Geophys. Res.* **88**, 6576 (1983).

19. Hegerl, G. C., Crowley, T. J., Baum, S. K., Kim, K.-Y. & Hyde, W. T. Detection of volcanic, solar, and greenhouse gas signals in paleo-

reconstructions of Northern Hemispheric temperature. *Geophys. Res. Lett.* **30** (5), 1242, doi:10.1029/2002GL016635 (2003).

20. Crowley, T. J., Baum, S. K., Kim, K-Y., Hegerl, G. C. & Hyde, W. T. Modeling ocean heat content changes during the last millennium. *Geophys. Res. Lett.*, **30** (18), 1932, doi:10.1029/2003GL017801 (2003).

21. Crowley, T. J & Kim, K.-Y. Modeling the temperature response to forced climate change over the last six centuries. *Geophys. Res. Lett.* **26**, 1901-1904 (1999).

22. Li, Y.-H., Peng, T.-H., Broecker, W. S. & Oestlund, H. G. The average vertical mixing coefficient for the oceanic thermocline. *Tellus* **36B**, 212-217 (1984).

23. Siegenthaler, U. Uptake of excess CO_2 by an outcrop-diffusion model of the ocean. *J. Geophys. Res.*, **88**, 3599 (1983).

24. Levitus, S., Antonov, J. & Boyer, T. Warming of the world ocean, 1955-2003.*Geophys. Res. Lett.* **32**, L02604, doi:10.1029/2004GL021592 (2005).

25. Free, M. & Robock, A. Global warming in the context of the little Ice Age. *J. Geophys. Res.* **104**, 19057-19070 (1999).

26. Stuiver, M. & Braziunas, T. F. Modeling atmospheric ^{14}C influence and ^{14}C ages of marine samples to 10,000 BC. *Radiocarbon* **35**, 137 (1993).

27. Lean, J. L., Beer, J. & Bradley, R. Reconstruction of solar irradiance changes since 1610: Implications for climate change. *Geophys. Res., Lett.* **22**, 3195 (1995).

28. Lean, J. L., Wang, Y.-M. & Sheeley, N. R. The effect of increasing solar activity on the Sun's total open magnetic flux during multiple cycles: Implications for solar forcing of climate. *Geophys. Res. Lett.* **29**, (24) 2224, doi:10.1029/2002GL015880 (2002).

29. Shindell, D.T., Schmidt, G.A., Mann, M.E. & Faluvegi, G. Dynamic winter climate response to large tropical volcanic eruptions since 1600. *J. Geophys. Res*. **109**, D05104, doi:10.1029/2003JD004151 (2004).

30. Thompson, D., Wallace, J. M. & Hegerl G. C. Annular modes in the extratropical circulation: Part II, Trends. *J. Climate*, **13**, 1018-1036 (2000).

Supplementary Information: see hegerletal_sens_SI.doc

Acknowledgements and author contributions: We thank Chris Forest for suggesting merging pdf estimates from results based on past-millenium climate changes with those based on 20th century climate change. The authors wish to thank Jesse Kenyon for technical support, and Myles Allen, Francis Zwiers, Alan Gelfand and Michael Lavine for very helpful discussions. We thank Chris Forest, Natalia Andronova, Reto Knutti and Jonathan Gregory for providing data, and three reviewers for their constructive suggestions. GH and TC were supported by NOAA and by NOAA's office of global programs and the DOE's office of Biological and Environmental research. GH was additionally supported by NSF. Author contributions: GH developed and implemented the method to estimate sensitivity and to calibrate proxy records. TC provided the reconstruction of past forcing and developed the CH-blend reconstruction, WH performed the EBM simulation, and DF derived the prior estimate of sensitivity from instrumental data 1950-2000.

Correspondence and requests for materials should be addressed to Gabriele Hegerl (e-mail: hegerl@duke.edu).

Figure 1: Paleoclimatic records [11-15] compared to a climate model simulation. CH-blend represents 30-90N annual mean temperature (shaded: 10% to 90% ranges for uncertainty in the amplitude of the reconstruction), Mann and Jones 0-90N, Esper et al. 30-90N land temperature and Briffa et al. 20-90N growing season temperature (dashed: reconstructions rescaled [15]). The model has a sensitivity of 2.5K, mid-range ocean diffusivity and is driven with mid-range aerosol forcing. All data are smoothed to focus on multi-decadal variability and shown as anomalies relative to the period prior to1800. The instrumental record for 30-90N annual mean surface temperature is offset to match CH-blend between 1880 to 1960.

Figure 2: Northern hemispheric mean radiative forcing. Sub-annual forcing data are used in the climate model simulations, a decadal filter is applied here for illustration only to focus on time-scales most relevant for the analysis. For tropospheric aerosol forcing (green), a range of forcing has been used, for solar and volcanic forcing, a best guess forcing (thick line) and a Gaussian uncertainty range has been used (2.5 and 97.5% limits shown by thin lines, lower limit for solar on zero-line). Greenhouse gas (" Ghg") and aerosol forcing are offset by 3 W/m ^{2}, and solar forcing by 1 W/m ^{2} for clarity.

Figure 3: Estimated probability densitity functions (pdfs) for equilibrium climate sensitivity to CO_2 doubling [K]. a) pdfs from a range of paleo reconstructions using data to 1850 (dotted: based on rescaled data). The horizontal bars indicate the 5-95% range of each pdf (median indicated by a dot and 10 th and 90th percentile by a vertical bar). b) comparison to other estimates of climate sensitivity based on instrumental data [3,4,6,7] over the 20 th century or 1950-2000 [8]. All pdfs have been scaled to integrate to 1 between 0 and 10 for better comparison. c) combined estimate from instrumental data [8] and proxy data.

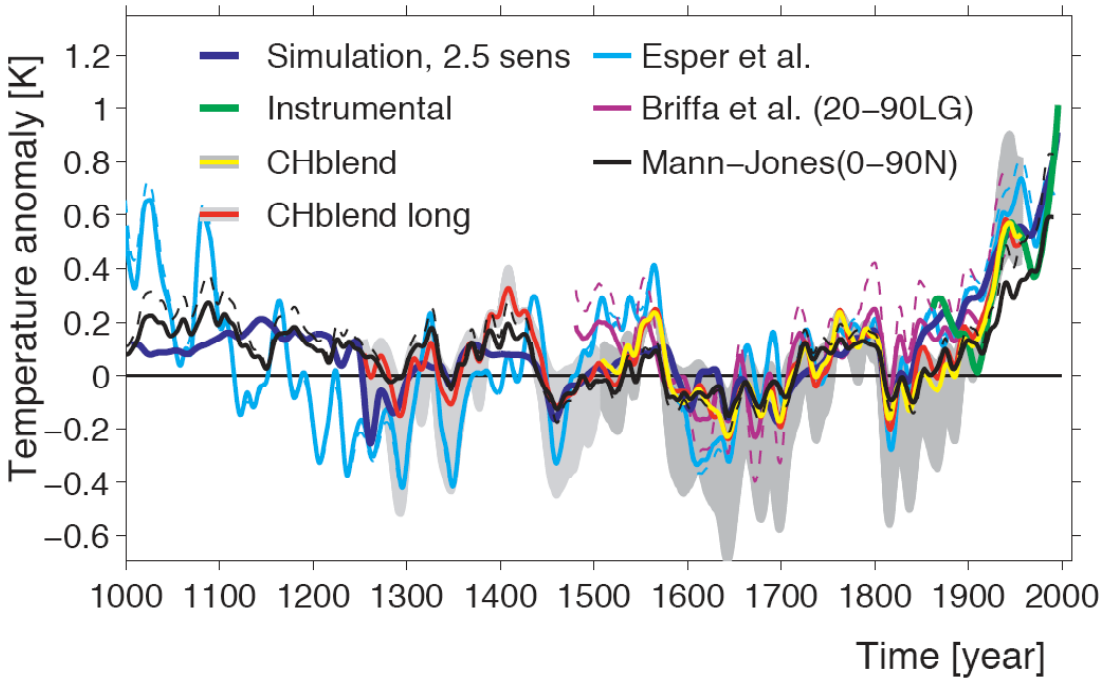
Simulation, 2.5 sens
Instrumental
CHblend
CHblend long
Esper et al.
Briffa et al. (20–90LG)
Mann–Jones(0–90N)
Temperature anomaly [K]
1.2
1
0.8
0.6
0.4
0.2
0
–0.2
–0.4
–0.6
1000
1100
1200
1300
1400
1500
1600
1700
1800
1900
2000
Time [year]

Figure 1

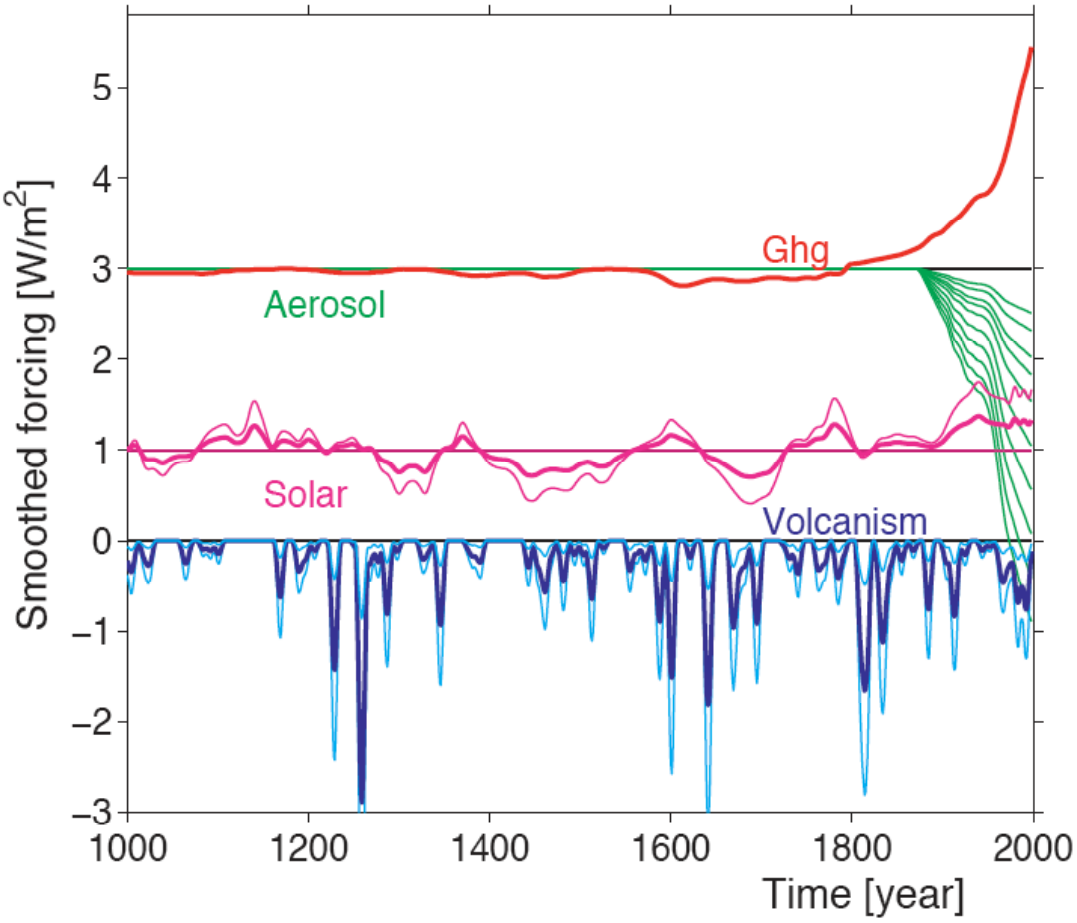
Smoothed forcing [W/m^2]
5
4
3
2
1
0
−1
−2
−3
1000
1200
1400
1600
1800
2000
Time [year]
Ghg
Aerosol
Solar
Volcanism

Figure 2

a)

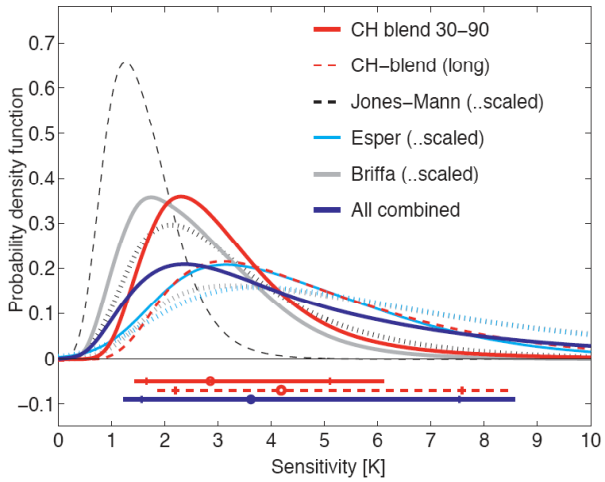
CH blend 30–90
CH–blend (long)
Jones–Mann (..scaled)
Esper (..scaled)
Briffa (..scaled)
All combined
Probability density function
Sensitivity [K]

b)

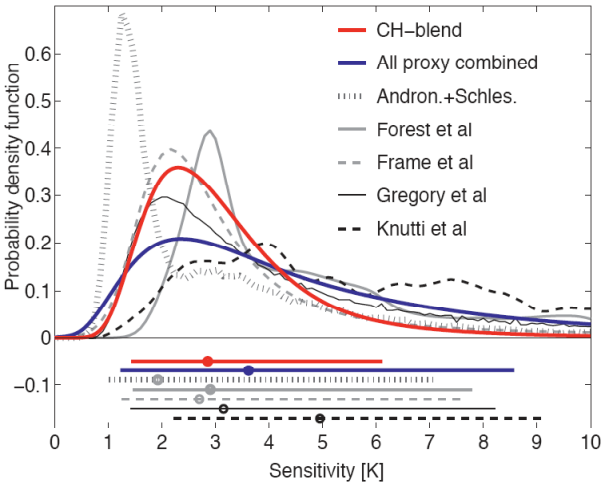
CH–blend
All proxy combined
Andron.+Schles.
Forest et al
Frame et al
Gregory et al
Knutti et al
Probability density function
Sensitivity [K]

c)

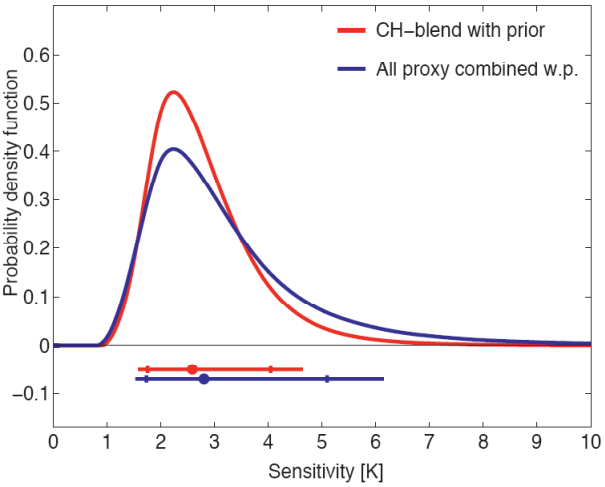
CH–blend with prior
All proxy combined w.p.
Probability density function
Sensitivity [K]

Figure 3